On the impact of lattice parameter accuracy of atomistic simulations on the microstructure of Ni-Ti shape memory alloys

Ia Rosa, Lorenzo; Maresca, Francesco

Published in:
Modelling and Simulation in Materials Science and Engineering

DOI:
10.1088/1361-651X/ac3b9e

PAPER

On the impact of lattice parameter accuracy of atomistic simulations on the microstructure of Ni–Ti shape memory alloys

To cite this article: L La Rosa and F Maresca 2022 *Modelling Simul. Mater. Sci. Eng.* **30** 014003

IOP Publishing Modelling and Simulation in Materials Science and Engineering
Modelling Simul. Mater. Sci. Eng. **30** (2022) 014003 (23pp) https://doi.org/10.1088/1361-651X/ac3b9e

On the impact of lattice parameter accuracy of atomistic simulations on the microstructure of Ni–Ti shape memory alloys

L La Rosa* **and F Maresca***

Engineering and Technology Institute, Faculty of Science and Engineering, University of Groningen, 9747 AG Groningen, The Netherlands

E-mail: l.la.rosa@rug.nl and f.maresca@rug.nl

Received 4 October 2021, revised 8 November 2021
Accepted for publication 19 November 2021
Published 7 December 2021

Abstract

Ni–Ti is a key shape-memory alloy (SMA) system for applications, being cheap and having good mechanical properties. Recently, atomistic simulations of Ni–Ti SMAs have been used with the purpose of revealing the nano-scale mechanisms that control superelasticity and the shape-memory effect (SME), which is crucial to guide alloying or processing strategies to improve materials performance. These atomistic simulations are based on molecular dynamics (MD) modelling that relies on (empirical) interatomic potentials (IAPs). These simulations must reproduce accurately the mechanism of martensitic transformation and the microstructure that it originates, since this controls both superelasticity and the SME. As demonstrated by the energy minimization theory of martensitic transformations (Ball and James (1987 *Arch. Ration. Mech. Anal.* **100** 13–52)), the microstructure of martensite depends on the lattice parameters of the austenite and the martensite phases. Here, we compute the bounds of possible microstructural variations based on the experimental variations/uncertainties in the lattice parameter measurements. We show that both density functional theory and MD lattice parameters are typically outside the experimental range, and that seemingly small deviations from this range induce large deviations from the experimental bounds of the microstructural predictions, with notable cases where unphysical microstructures are predicted to form. Therefore, our work points to a strategy for benchmarking and selecting IAPs for atomistic modelling of SMAs, which is crucial to modelling the development of martensitic microstructures and their impact on the SME.

*Authors to whom any correspondence should be addressed.

Keywords: Ni–Ti, shape memory alloys, martensite, molecular dynamics

S Supplementary material for this article is available online

(Some figures may appear in colour only in the online journal)

Introduction

Since Ölander (1932) revealed the shape-memory effect (SME) in Au–Cd samples, shape memory alloys (SMAs) have attracted significant attention and interest both for their surprising behaviour and for the possibly wide range of engineering applications such as structures and composites (Furuya 1996), actuators in automotive applications (Stoeckel 1990, Leo *et al* 1998, Jani *et al* 2014) and robotics (Furuya and Shimada 1991, Sreekumar *et al* 2007, Kheirikhah *et al* 2010), aircraft morphing in aerospace design (Schetky 1991, Hartl and Lagoudas 2007, Bil *et al* 2013), mini actuators and micro-electromechanical systems (Kahn *et al* 1998, Fujita and Toshiyoshi 1998, Van Humbeeck 1999), devices for minimally invasive surgery in biomedical applications (Duerig *et al* 1999, Mantovani 2000, Machado and Savi 2003, Morgan 2004, Song 2010, Petrini and Migliavacca 2011) and industrial applications such as eyeglass frames (Zider and Krumme 1988, Hautcoeur and Eberhardt 1997, Wu and Schetky 2000). When an external stimulus (stress or temperature) is applied, SMAs undergo a martensitic transformation that results in microstructural changes (Otsuka and Ren 2005). Upon removal of the external stimulus, the transformation and the microstructural changes are reversed and the original shape of the material is recovered, hence the name. Ni–Ti SMAs are cheaper than other SMAs and have been key to the engineering and industrial use of SMAs since the work of Buehler *et al* (1963) revealed their shape memory behaviour. The Ni–Ti phase diagram (e.g. Otsuka and Kakeshita (2002)) shows a narrow region near the equiatomic composition at finite temperatures (approximately between 627 and 1090°C), where the system shows a stable cubic B2 phase, i.e. the austenite. Upon quenching, this B2 structure transforms into the monoclinic B19′ martensite (Otsuka *et al* 1971a, Hehemann and Sandrock 1971), yet some B2 austenite can be retained (Otsuka and Ren 2005). This is a single-step transformation, yet, different transformation paths, involving intermediate rhombohedral (R) and orthorhombic (B19) phases, can also be achieved, however, in the ternary Ni–Ti-based alloys, which are beyond the scope of this paper (Otsuka and Ren 2005).

The microstructure of martensite consists of several symmetry-related martensite variants that originate from common austenite crystals. The austenite-to-martensite transformation typically involves significant volumetric changes and large shear strains, thus the martensite variants can pair to form twinning systems that can self-accommodate such a shape change. Continuum models like the energy minimization theory (EMT, Ball and James (1987)) enable the prediction of the twinning systems as a function of only the lattice parameters of the austenite and the martensite. In the literature, a large number of experimental observations on Ni–Ti systems are available (Laves and Wallbaum 1939, Duwez and Taylor 1950, Philip and Beck 1957, Purdy and Parr 1960, Dautovich and Purdy 1965, De Lange and Zijderveld 1968, Otsuka *et al* 1971b, 1971a, Hehemann and Sandrock 1971, Monasevich *et al* 1979, Monasevich and Paskal 1980, Tadaki and Wayman 1980, Michal and Sinclair 1981, Buhrer *et al* 1983, Kudoh *et al* 1985, Nishida *et al* 1988, 1995a, 1995b, Prokoshkin *et al* 2004) and well-established theories such as the phenomenological theory of martensite crystallography (Wayman 1994, Bhadeshia and Wayman 2014) and EMT (Ball and James 1987, Bhattacharya 1992) have been successfully used to describe the martensitic microstructure, including the twinning systems

and the habit planes (Knowles and Smith 1981, Matsumoto *et al* 1987, Onda *et al* 1992, Hane and Shield 1999, Sehitoglu *et al* 2000).

Recently, atomistic simulations have been performed to reveal the nanoscale mechanisms that control martensite formation and twinning. In the context of Ni–Ti, both density functional theory (DFT) and molecular dynamics (MD) studies have been performed over the past few years. DFT modelling has been mostly focusing on the prediction of the transformation path (e.g. Hatcher *et al* (2009a), Holec *et al* (2011)), the structural stability of the crystalline phases (Hatcher *et al* 2009b, Vishnu and Strachan 2010), the size effects (Vishnu and Strachan 2012) and the energy barriers of the highly symmetric compound twins (Ezaz *et al* 2011). However, since DFT simulations are restricted to a few hundred atoms, larger systems are typically modeled by using MD (e.g. Ko *et al* (2015), Ren and Sehitoglu (2016), Kim *et al* (2017), Srinivasan *et al* (2019), Kavousi *et al* (2019)). The typical approach for developing interatomic potentials (IAPs) is based on selecting some empirical formalism, e.g. the embedded atom method (EAM) (Daw and Baskes 1984) and the modified EAM (MEAM) (Baskes 1992), and fit the potential parameters to a set of properties (from experiments and/or from DFT), such as the lattice parameters and the elastic constants. However, depending on the fitting procedure and the settings of the DFT calculations, discrepancies between the atomistic lattice parameters and the experimental ones typically occur. In fact, while EMT reveals the critical dependence of the microstructure of martensite (i.e. twinning systems and habit planes) on these lattice parameters, the existing atomistic literature does not discuss this dependence and hence it is unclear whether the lattice parameters of atomistic simulations are 'accurate enough' to provide reasonable/physically sound descriptions of the microstructure of martensite.

In this work, the dependence of microstructure on the lattice parameter accuracy is analysed for Ni–Ti SMAs. First (section 2) the experimental measurements are considered of the B2 and B19′ lattice parameters and monoclinic angle and their variability is determined with respect to temperature and compositional changes around the equiatomic range, which is relevant for Ni–Ti SMAs. Next (section 3), EMT is used to assess the possible uncertainty range of the shape deformation in Ni–Ti, based on the experimental variability and uncertainties. In section 4, DFT and MD predictions of the lattice parameters and monoclinic angles are compared with the experimental range, and EMT is used to predict the shape deformation based on the existing DFT data and MD IAPs. The paper ends with discussion and conclusions.

Here, the following notation is used. Lowercase letters are scalars. Bold lowercase letters denote vectors. Bold Latin capital letters denote second order tensors, where $\mathbf{I}$ is the identity. Given a second order tensor $\mathbf{A}$, then tr($\mathbf{A}$) and det($\mathbf{A}$) denote the trace and the determinant of the tensor, respectively, while the superscripts $\mathbf{A}^{\mathrm{T}}$ and $\mathbf{A}^{-1}$ denote the transpose and the inverse of the tensor, respectively. The '$\cdot$'product contracts one component of a tensor with a component of another tensor, i.e. $(\mathbf{A}\cdot\mathbf{B})_{ij}=\mathbf{A}_{ik}\mathbf{B}_{kj}$, where the Einstein summation convention applies. In the case of two vectors $\mathbf{a}$ and $\mathbf{b}$, the '$\cdot$'product is the usual scalar product, defined as $\mathbf{a}\cdot\mathbf{b}=a_ib_i$. The tensor product is written as $\mathbf{a}\otimes\mathbf{b}$, which has components $(\mathbf{a}\otimes\mathbf{b})_{ij}=a_ib_j$. In the following, we will use the convention introduced by Bilby and Crocker (1965) for the twinning elements, hence the shear directions η_1,η_2 and the Twin planes normal K_1,K_2 are vectors.

1. Experimental bounds of Ni–Ti lattice parameters

Since Laves and Wallbaum (1939) clarified experimentally the B2 crystal structure of the austenite phase, it took more than a decade to obtain a first rough estimate of the austenite

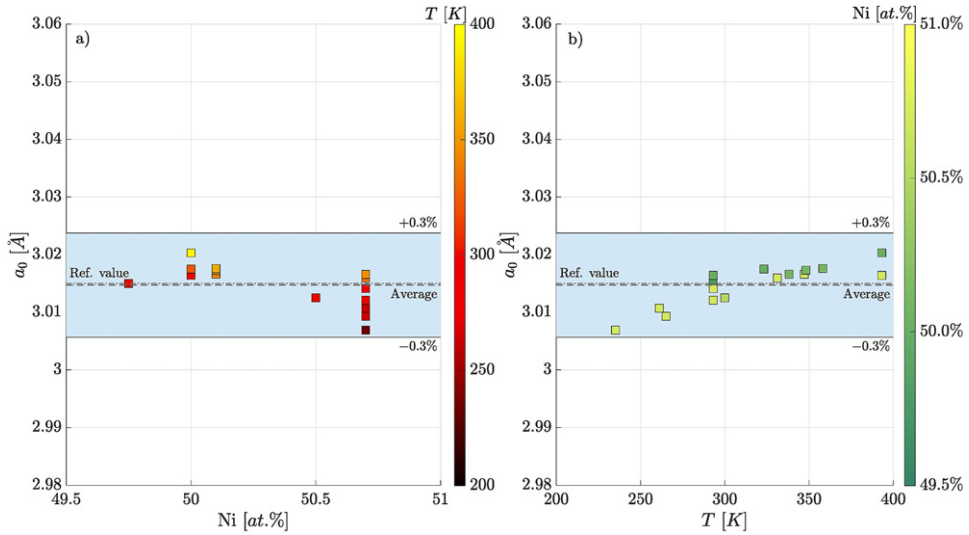

Figure 1. Dependence of the lattice parameter of the B2 austenite on (a) the Ni concentration and (b) temperature.

lattice parameter ($a_0 = 2.980$ Å) by Duwez and Taylor (1950). This estimate was later corrected to $a_0 = 3.015$ Å (Philip and Beck (1957)) and this is the reference, literature value for the austenitic B2 cell of an equiatomic Ni–Ti alloy. The lattice parameter can clearly vary depending on the temperature and the alloy composition. Figure 1 shows the dependence of the lattice parameter on the alloy composition and temperature. The literature data are summarized in table 5 in the appendix. It appears that the B2 lattice parameter is well contained within $\pm 0.3\%$ error from the average value $a_0 = 3.0147$ Å, irrespective of the detailed composition and measurement temperature (figure 1).

Unlike the austenite, the martensite crystal structure remained a mystery for a long time, since its first report by Purdy and Parr (1960) as an hexagonal crystal. Shortly after, by using electron diffraction and x-ray powder diffraction method, Dautovich and Purdy (1965) reported a triclinic crystal structure for an heat-treated Ni–Ti alloy, with chemical composition of 51% at. Ni, whose lattice parameters were $a = 2.860$ Å, $b = 4.110$ Å, $c = 4.6$ Å, $\alpha = 90.1°$, $\beta = 96.7°$, $\gamma = 90.9°$. However, the B19′ crystal structure was only reported for the first time by Otsuka *et al* (1971a) and Hehemann and Sandrock (1971) independently, who reported the same monoclinic structure with almost the same lattice parameters $a = 2.889$ Å, $b = 4.120$ Å, $c = 4.622$ Å, $\beta = 96.8°$ (Otsuka *et al* 1971a) and $a = 2.883$ Å, $b = 4.117$ Å, $c = 4.623$ Å, $\beta = 96.8°$ (Hehemann and Sandrock 1971). The only differences between the two structures were the space group operation and the position of the atoms within the crystal cell. These differences were due to different direction and plane of the atomic shuffles, relative to the monoclinic angle, which led Otsuka *et al* (1971a) to the wrong $P2/c$ space group instead of the correct $P2_1/m$ space group reported by Hehemann and Sandrock (1971). However, the positions of the atoms within the crystal cell, as envisioned by Hehemann and Sandrock (1971), were incorrect. After several attempts (e.g. Michal and Sinclair (1981)), the correct structure was discovered by Kudoh *et al* (1985), who reported a monoclinic B19′ martensite with lattice parameters $a = 2.898$ Å, $b = 4.108$ Å, $c = 4.646$ Å, $\beta = 97.78°$, for an alloy with a chemical composition of 49.2% at. Ni. More recently, Prokoshkin *et al* (2004) conducted an in-depth

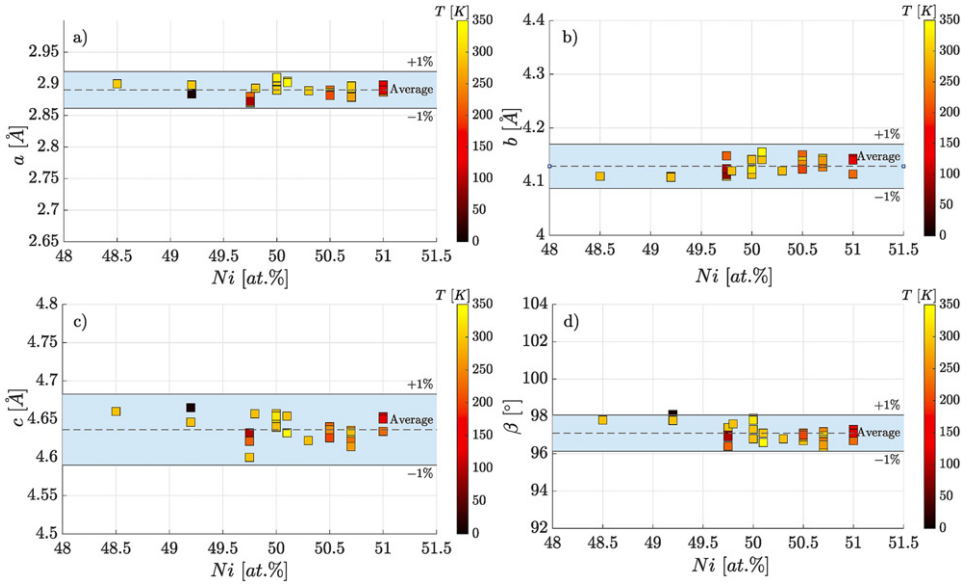

Figure 2. Dependence of the (a) a, (b) b, (c) c lattice parameters and the (d) monoclinic angle β on the Ni concentrations. The color-bar shows the observation temperature of the B19′ martensite.

study of the lattice parameters of the martensitic phase in the equiatomic Ni–Ti system, collecting a large amount of experimental data from the literature and performing further experiments, in order to find correlations between temperature or chemistry and trends in lattice parameter changes. Prokoshkin *et al* (2004) concluded that, in the nearly equiatomic nickel-concentration range of binary Ni–Ti alloys, the lattice parameters a, c and the monoclinic angle β decrease, while the parameter b increases as Ni increases. Also, Prokoshkin *et al* (2004) analyzed the temperature dependencies of the B19′ martensite lattice parameters. They concluded that in general, as temperature increases, the parameter a slightly increases, b increases while c and β decrease.

Here, we collected a large amount of crystallographic data (Dautovich and Purdy 1965, De Lange and Zijderveld 1968, Otsuka *et al* 1971a, 1971b, Hehemann and Sandrock 1971, Monasevich and Paskal 1980, Tadaki and Wayman 1980, Michal and Sinclair 1981, Buhrer *et al* 1983, Savvinov *et al* 1984, Kudoh *et al* 1985, Khachin *et al* 1992, Mironov and Kul'Kov 1994, Gundyrev *et al* 1999, Sittner *et al* 2003, Prokoshkin *et al* 2004, Khalil-Allafi *et al* 2004) and plotted the measured lattice parameters as a function of the chemistry and the temperature (figure 2 and 3). The data are listed in table 6 in the appendix.

Figures 2 and 3 confirm the trends reported by Prokoshkin *et al* (2004), however, the changes in lattice parameter and monoclinic angle are well contained within $\pm 1\%$ deviation from the average. This order of fluctuations should be close to the experimental accuracy with which the lattice parameters have been measured. To verify this, we consider two sets of lattice parameters, shown in table 1, that have been extracted based on the same experimental data but analyzed with slightly different approaches by Otsuka *et al* (1971a) and by Prokoshkin *et al* (2004). The volume change is also reported, which is determined as

$$\frac{\Delta V}{V_0} = \frac{abc}{2a_0^3} \sin \beta - 1. \tag{1}$$

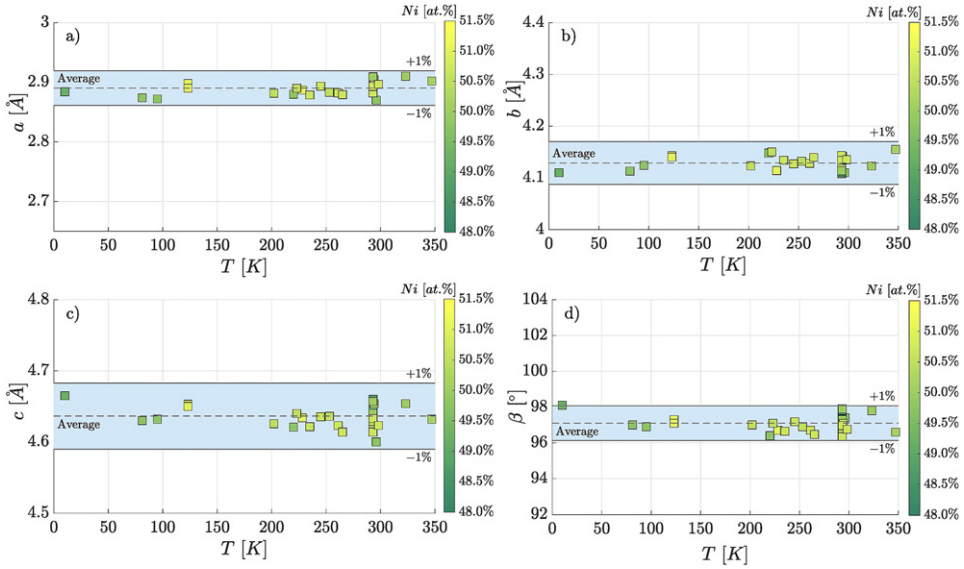

Figure 3. Dependence of the (a) a, (b) b, (c) c lattice parameters and the (d) monoclinic angle β on the observation temperature. The color-bar shows the Ni concentration of the B19′ martensite.

Table 1. Differences between the estimated lattice parameters made by Otsuka *et al* (1971a) and the refined values recalculated by Prokoshkin *et al* (2004) (Otsuka *et al* (1971a) ⋆).

	a_0 (Å)	a (Å)	b (Å)	c (Å)	β (°)	$\Delta V/V_0$(%)
Otsuka *et al* (1971a)	3.015	2.889	4.120	4.622	96.8	−0.34
Otsuka *et al* (1971a) ⋆	3.015	2.874	4.113	4.630	97.0	−0.90
	—	0.52%	0.17%	0.17%	0.21%	0.56%

This order of fluctuations, that we could expect from experimental measurements, is very small and, therefore, we can conclude that the trends found by Prokoshkin *et al* (2004) on the lattice parameters, for nearly equiatomic Ni–Ti alloy, do not depend strongly on the chemical composition nor the observation temperature and the measured dependencies on the composition and temperature are of the order of the experimental accuracy.

2. Theory bounds for martensitic microstructures in Ni–Ti

2.1. Twinning systems

Martensite variants arrange to form twinning systems, in order to self-accommodate the shape change due to the transformation. The twinning systems are defined by the twinning shear s, the shear direction η_1 and the twin plane normal K_1. The triplet (s, η_1, K_1) is the twinning mode. According to Bilby and Crocker (1965), the simple shear deformation, that involves a twin structure, leaves also a second undistorted (but rotated) plane K_2 and a second direction η_2. The pair (K_2, η_2) represent a conjugate (or reciprocal) twinning mode that has the same

shear magnitude s. The twinning systems are usually classified as type I twins (rational twin plane), type II twins (rational shear direction), and compound twins (both twin plane and shear directions rational). Here, we summarize the main EMT model equations to determine the twinning systems as a function of the B2 and B19′ lattice parameters and monoclinic angle.

The twinned martensite microstructure is the result of a continuous deformation, hence two distinct B19′ variants can form a variant pair if the following compatibility condition is satisfied (Ball and James 1987, Bhattacharya 1992)

$$\mathbf{Q}\cdot\mathbf{B}_I-\mathbf{B}_J=\mathbf{a}\otimes\mathbf{n}, \tag{2}$$

where $\mathbf{n}$ is the normal to the twin plane, $\mathbf{a}$ is the shear vector, $\mathbf{Q}$ is a rotation tensor and $\mathbf{B}_I$ and $\mathbf{B}_J$ are the Bain strains of the I and J variants. Equation (2) is also known as *twinning equation* and its solution was obtained by Ball and James (1987). Solutions to equation (2) can be obtained by using Mallard's law (Bhattacharya 1992), according to which $\mathbf{B}_I=\mathbf{R}^{\mathrm{T}}\cdot\mathbf{B}_J\cdot\mathbf{R}$, where $\mathbf{R}$ is a 180° rotation about an axis $\mathbf{i}$ of the austenite lattice, in which case

$$\begin{aligned}\mathbf{a}_{\mathrm{I}}&=2\left(\frac{\mathbf{B}_J^{-\mathrm{T}}\cdot\mathbf{i}}{|\mathbf{B}_J^{-\mathrm{T}}\cdot\mathbf{i}|^2}-\mathbf{B}_J\cdot\mathbf{i}\right)\quad\text{and}\quad\mathbf{n}_{\mathrm{I}}=\mathbf{i},\\ \mathbf{a}_{\mathrm{II}}&=\rho\mathbf{B}_J\cdot\mathbf{i}\quad\text{and}\quad\mathbf{n}_{\mathrm{II}}=\frac{2}{\rho}\left(\mathbf{I}-\frac{\mathbf{B}_J^{\mathrm{T}}\cdot\mathbf{B}_J}{|\mathbf{B}_J\cdot\mathbf{i}|^2}\right)\cdot\mathbf{i},\end{aligned} \tag{3}$$

where $\rho\neq0$ is such that $|\mathbf{n}|=1$. It is customary to express the solutions of equation (3) with respect to the martensite lattice on one side of the twin and hence the twinning elements can be computed as

$$K_1=\frac{\mathbf{B}_J^{-1}\cdot\mathbf{n}_{\mathrm{I}}}{|\mathbf{B}_J^{-1}\cdot\mathbf{n}_{\mathrm{I}}|},\quad\eta_1=\frac{\mathbf{a}_{\mathrm{I}}}{|\mathbf{a}_{\mathrm{I}}|},\quad K_2=\frac{\mathbf{B}_J^{-1}\cdot\mathbf{n}_{\mathrm{II}}}{|\mathbf{B}_J^{-1}\cdot\mathbf{n}_{\mathrm{II}}|},\quad\eta_2=\frac{\mathbf{a}_{\mathrm{II}}}{|\mathbf{a}_{\mathrm{II}}|}, \tag{4}$$

and

$$K_1=\frac{\mathbf{B}_J^{-1}\cdot\mathbf{n}_{\mathrm{II}}}{|\mathbf{B}_J^{-1}\cdot\mathbf{n}_{\mathrm{II}}|},\quad\eta_1=\frac{\mathbf{a}_{\mathrm{II}}}{|\mathbf{a}_{\mathrm{II}}|},\quad K_2=\frac{\mathbf{B}_J^{-1}\cdot\mathbf{n}_{\mathrm{I}}}{|\mathbf{B}_J^{-1}\cdot\mathbf{n}_{\mathrm{I}}|},\quad\eta_2=\frac{\mathbf{a}_{\mathrm{I}}}{|\mathbf{a}_{\mathrm{I}}|}. \tag{5}$$

For both solutions, the twinning shear is

$$s=|\mathbf{a}_{\mathrm{I}}||\mathbf{B}_J^{-1}\cdot\mathbf{n}_{\mathrm{I}}|=|\mathbf{a}_{\mathrm{II}}||\mathbf{B}_J^{-1}\cdot\mathbf{n}_{\mathrm{II}}|. \tag{6}$$

In equation (4), K_1 and η_2 are rational crystallographic directions, hence this solution is a type I twin. Equation (5) describes a type II twin, because η_1 and K_2 are rational crystallographic directions. At last, if all four of the twinning elements are rational, then both twins are compound twins. As discussed e.g. in Bhattacharya (2003) and shown by Hane and Shield (1999), equation (3) yields all possible twinning systems for Ni–Ti.

2.2. Austenite–martensite habit plane

EMT can also predict the crystallography of the austenite–martensite interface (habit plane) (Ball and James 1987). In Ni–Ti, a compatible interface between austenite and one single variant cannot be obtained. Therefore, the austenite crystal forms a compatible interface with a laminate that consists of alternating twins. Ball and James (1987) proved that, for infinitely fine twins, the austenite–martensite interface energy goes to zero if and only if the habit plane can form a compatible interface with the average deformation

$$\mathbf{F}_\lambda=\lambda\mathbf{Q}\cdot\mathbf{B}_I+(1-\lambda)\mathbf{B}_J, \tag{7}$$

where $\lambda \in (0,1)$ is the twin volume fraction and $\mathbf{Q}$ is the rotation tensor introduced in equation (2). Then, a finely twinned microstructure can form an interface with the austenite if

$$\hat{\mathbf{Q}} \cdot (\lambda \mathbf{Q} \cdot \mathbf{B}_I + (1-\lambda)\mathbf{B}_J) - \mathbf{I} = \mathbf{b} \otimes \mathbf{m}. \tag{8}$$

where $\mathbf{b}$ is the vector setting the direction and magnitude of the shape deformation, $\mathbf{m}$ is the habit plane normal and $\hat{\mathbf{Q}}$ is a rotation tensor. Equation (8) is the *austenite–martensite interface equation* and it gives solutions if the the twinning equation (2) can be solved for a given variant pair (I, J). Ball and James (1987) proved that equation (8) has solutions if and only if the following conditions are met

$$\begin{aligned} \delta &= \mathbf{a} \cdot \mathbf{B}_J \cdot (\mathbf{B}_J^2 - \mathbf{I})^{-1} \cdot \mathbf{n} \leqslant -2, \\ \eta &= \mathrm{tr}(\mathbf{B}_J^2) - \det(\mathbf{B}_J^2) - 2 + \frac{|\mathbf{a}|^2}{2\delta} \geqslant 0, \end{aligned} \tag{9}$$

where $\mathbf{B}_J^2 = \mathbf{B}_J^{\mathrm{T}} \cdot \mathbf{B}_J$. If equations (9) are satisfied, then solutions can be computed for the twin volume fractions

$$\lambda = \frac{1 - \sqrt{1 + \frac{2}{\delta}}}{2}, \tag{10}$$

and $\lambda^* = 1 - \lambda$. Once the twin volume fractions are known, Ball and James (1987) showed that the solutions to the austenite–martensite interface are

$$\begin{aligned} \mathbf{b} &= \rho \left(\sqrt{\frac{\lambda_3(1-\lambda_1)}{\lambda_3 - \lambda_1}} \mathbf{v}_1 \pm \sqrt{\frac{\lambda_1(\lambda_3 - 1)}{\lambda_3 - \lambda_1}} \mathbf{v}_3 \right), \\ \mathbf{m} &= \frac{\sqrt{\lambda_3} - \sqrt{\lambda_1}}{\rho\sqrt{\lambda_3 - \lambda_1}} (-\sqrt{1-\lambda_1}\mathbf{v}_1 \pm \sqrt{\lambda_3 - 1}\mathbf{v}_3), \end{aligned} \tag{11}$$

where ρ is chosen such that $|\mathbf{m}| = 1$ and $\mathbf{v}_\Gamma$, with $\Gamma = 1, 2, 3$, are the eigenvectors of the symmetric tensor

$$\mathbf{C}_\lambda = (\mathbf{B}_J + \lambda \mathbf{n} \otimes \mathbf{a}) \cdot (\mathbf{B}_J + \lambda \mathbf{a} \otimes \mathbf{n}), \tag{12}$$

with eigenvalues $\lambda_1 \leqslant 1$, $\lambda_2 = 1$ and $\lambda_3 \geqslant 1$.

EMT has been successfully applied, through the years, to explain the observed martensite microstructures (Bhattacharya 1992). The solutions of equations (2) and (8), in the case of Ni–Ti, have been reported by Hane and Shield (1999) and Sehitoglu *et al* (2000), who predicted 42 independent twinning systems, distinguished in four modes (A, B, C and D), and 192 habit planes. Next, we will show the predictions for type II mode B twins, which are the most observed in experiments, and we will show the sensitivity of the solutions to equations (2) and (8) with respect to the uncertainties in the experimental lattice parameters.

2.3. Theory bounds for twinning and habit planes

As discussed in the literature (Hane and Shield 1999, Bhattacharya 2003), the type II mode B twin volume fraction predictions, with Otsuka *et al* (1971a) lattice parameters, are close to the the experimental observation (relative error 1.62%), (Onda *et al* 1992). Moreover, deviations from experiments (Matsumoto *et al* 1987) of the habit plane normal $\mathbf{m}$ and the shape strain $\mathbf{b}$ are 3.58° and 1.90°, respectively.

Table 2. Sensitivity of the results of equations (2) and (8) in nearly equiatomic Ni–Ti martensitic transformation, by using as input the lattice parameters reported by Otsuka *et al* (1971a) and the ones reanalyzed by Prokoshkin *et al* (2004) (Otsuka *et al* (1971a) ⋆).

$\mathbf{a}_{\mathrm{II}}$	$\mathbf{n}_{\mathrm{II}}$	s	reference
$(\overline{0.0120}\ 0.289\ 00.0164)$	$(0.5846\ 0\ \overline{0.8113})$	0.2804	Otsuka *et al* (1971a)
$(\overline{0.0127}\ 0.2972\ 0.0173)$	$(0.5830\ 0\ \overline{0.8125})$	0.2886	Otsuka *et al* (1971a) ⋆
$//0.12^\circ$	$//0.11^\circ$	2.85%	
$\mathbf{b}^-$	$\mathbf{m}^-$	λ	reference
$(\overline{0.0554}\ \overline{0.0619}\ \overline{0.1010})$	$(0.8977\ \overline{0.3775}\ \overline{0.2272})$	0.2710	Otsuka *et al* (1971a)
$(\overline{0.0612}\ \overline{0.0633}\ \overline{0.1033})$	$(0.9023\ \overline{0.3700}\ \overline{0.2211})$	0.2770	Otsuka *et al* (1971a) ⋆
$//1.74^\circ$	$//0.62^\circ$	2.16%	

Table 3. Set of measurements of B2 and B19′ lattice parameters used as input for predictions.

	a_0 (Å)	a (Å)	b (Å)	c (Å)	β (°)	$\Delta V/V_0$(%)
Otsuka *et al* (1971a)	3.015	2.889	4.120	4.622	96.80	−0.34
Sittner *et al* (2003)	3.013	2.882	4.123	4.626	97.00	−0.24
Prokoshkin *et al* (2004)[1]	3.0175	2.9100	4.1230	4.6540	97.80	+0.68
Prokoshkin *et al* (2004)[2]	3.0164	2.9090	4.1135	4.6570	97.90	+0.56
Prokoshkin *et al* (2004)[3]	3.0107	2.8820	4.1280	4.6230	96.70	+0.08
Prokoshkin *et al* (2004)[4]	3.0121	2.8820	4.1430	4.6140	96.35	+0.18
Khalil-Allafi *et al* (2004)[1]	3.0141	2.893	4.134	4.633	96.96	+0.43
Khalil-Allafi *et al* (2004)[2]	3.0069	2.8786	4.1340	4.6215	96.65	+0.47
Khalil-Allafi *et al* (2004)[3]	3.0093	2.8792	4.1394	4.6140	96.47	+0.25

By using the input lattice parameters of table 1 to solve equations (2) and (8), the type II mode B twinning system and the related habit plane are obtained, as reported in table 2.

As we can see, uncertainties in the lattice parameters do not yield apparent changes in the orientation of the twin and habit plane, since the deviations between the shear vector (0.12°), twin plane normal (0.11°), shape strain (1.74°) and habit plane normal (0.62°) are negligible. Small differences are also observed for the twinning shear (2.85%) and the twin volume fraction (2.16%). All in all, differences due to the lattice parameter accuracy yield discrepancies of predictions in the order of the mismatch between EMT and experiments, which is thus limited.

We now assess the degree of accuracy that can be expected when predicting twinning systems and the austenite–martensite interface, by considering the experimental ±1% scatter in the measurements of the lattice parameters. To this purpose, we consider as experimental input those references that provide a complete set of lattice parameters of both B2 and B19′, see table 3.

Figure 4 shows the theory predictions (equations (2) and (8)) for the type II mode B twinning system, which is the most frequently observed twinning system in Ni–Ti, and for which there are experimental measurements to compare the EMT predictions with (Matsumoto *et al* 1987, Onda *et al* 1992).

The predicted volume changes fall within ±1% accuracy range. The twin volume fraction λ shows a ±9% accuracy range. Note that the measurement of Onda *et al* (1992) is within this range. Finally, the predicted twinning shear s and shape strain magnitude $|b|$ fall within a

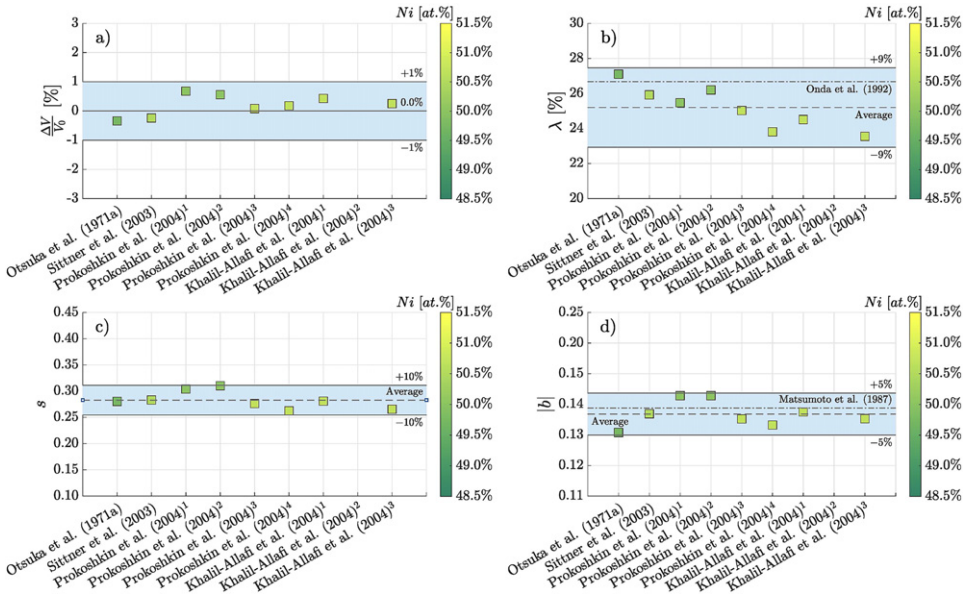

Figure 4. EMT predictions of (a) the volume change, (b) the twin volume fraction, (c) the twinning shear and (d) the shape strain magnitude by using lattice parameters taken from experiments. Here only the result for type II mode B twinning system are shown.

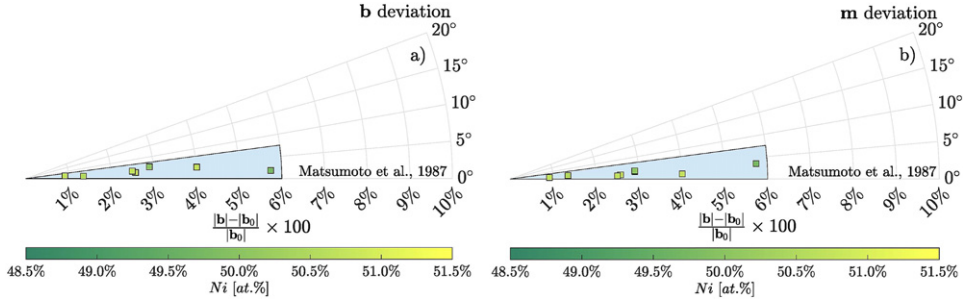

Figure 5. Deviation of the predicted (a) shape strain direction and magnitude and (b) of the habit plane normal direction and shape strain magnitude, based on the experimental lattice parameters, compared with (Matsumoto *et al* 1987) measurements. $|\mathbf{b}_0|$ is the Matsumoto *et al* (1987) shape strain magnitude.

$\pm 10\%$ and $\pm 5\%$ accuracy range, respectively. The magnitude of the shape strain measured by Matsumoto *et al* (1987) is very close to the average of the plotted data.

Figure 5 shows the deviations between predicted habit plane orientations or shape strain and the data by Matsumoto *et al* (1987). The data are plotted in a polar diagram where the radial coordinate is the relative difference, in absolute value, between the predicted shape strain and Matsumoto *et al* (1987) magnitudes while the angular coordinates are the deviations of **b** and **m** from Matsumoto *et al* (1987) habit plane measurements.

EMT, with Otsuka *et al* (1971b) lattice parameters, predicts an habit plane with deviations of 1.90°, for the shape strain direction, and 3.58°, for the habit plane normal. Sittner *et al* (2003)

lattice parameters give deviations, for the shape strain direction and habit plane normal, of 2.49° and 3.29°, respectively. Finally, Prokoshkin *et al* (2004) data show average deviations, for the shape strain direction and habit plane normal, respectively of 4.49° and 2.78°, while Khalil-Allafi *et al* (2004) data show an average habit plane deviation of the order of 4.03° (shape strain direction) and 1.80° (habit plane normal). With respect to Matsumoto *et al* (1987) observation, figure 5 shows that the predictions of the habit plane are well contained within 6% and 7.5°, for the shape strain magnitude error and habit plane deviation, respectively.

This analysis points out that seemingly small inaccuracies in the input lattice parameter, within the order of the experimental inaccuracies (±1%), can lead to measurable differences in twinning and habit plane predictions. With this result in mind, we turn our analysis to the predictions based on the lattice parameters obtained with atomistic modelling methods (DFT and MD).

3. Microstructural predictions based on atomistic input

To the best of the authors' knowledge, the first IAPs for Ni–Ti alloys were developed by Farkas *et al* (1996) and by Lai and Liu (2000). The first one is based on the EAM (Daw and Baskes (1984)), while the second one on the Finnis–Sinclair (FS) model (Finnis and Sinclair 1984). Mutter and Nielaba (2010) showed that these potentials are not able to reproduce the martensitic phase transformation, because they were developed to study the properties of the ternary Ni–Ti–Al alloy (Farkas *et al* 1996) and amorphous alloys (Lai and Liu 2000). Subsequently, two more potentials, based on the MEAM (Baskes (1992)), were developed by Saitoh *et al* (2010) and Ishida and Hiwatari (2007) for studying phase transitions in Ni–Ti. Again, Mutter and Nielaba (2010) showed that they do not reproduce convincingly neither the reversible temperature and stress-induced phase transitions nor the crystallography of the phases. More recently, Mutter and Nielaba (2010) and Zhong *et al* (2011) modified independently the FS potential by Lai and Liu (2000) and showed the occurrence of a reversible temperature-induced phase transition. However, their simulations showed atomic shuffles of the martensite structure in disagreement with the experiments. The wrongly predicted martensite structure led Mutter and Nielaba (2010) to predict the martensitic transition without the occurrence of any twinning, and Zhong *et al* (2011) to predict an unphysical twinning behavior with a negative twin boundary energy.

A significant step forward in the development of IAPs for Ni–Ti alloys is due to the recent work of Ko *et al* (2015). Ko *et al* (2015) developed an IAP based on the second nearest-neighbor (2NN) MEAM, that can reproduce not only the B2–B19′ martensitic transformation but also the properties of other phases. Recently, Srinivasan *et al* (2017) showed that the IAPs based on the 2NN-MEAM formalism (Ko *et al* 2015, Muralles *et al* 2017, Kim *et al* 2017, Kavousi *et al* 2019) perform better than the ones based on the EAM or FS formalisms (Lai and Liu 2000, Mutter and Nielaba 2010, Zhong *et al* 2011, Ren and Sehitoglu 2016), because they can predict more accurately the lattice parameters and elastic constants of both B2 and B19′ phases. However, Srinivasan *et al* (2019) pointed out that the 2NN-MEAM potentials present some non-negligible issues, such as the elastic constants of the martensitic phase that differ by up to 300% from the experimental data, along with inaccurate prediction of the transformation temperatures. Therefore, Srinivasan *et al* (2019) developed a potential based on the reference-free (RF) MEAM (Timonova and Thijsse 2010), where a broader dataset can be used for fitting compared with 2NN-MEAM. In addition to the 0 K energies, also finite temperature energies, atomic forces and stress tensors have been included.

Figures 6 and 7 show the DFT (Hatcher *et al* 2009a, 2009b, Vishnu and Strachan 2010, Holec *et al* 2011, Ko *et al* 2015, Srinivasan *et al* 2019) and MD IAPs (Ko *et al* 2015, Ren

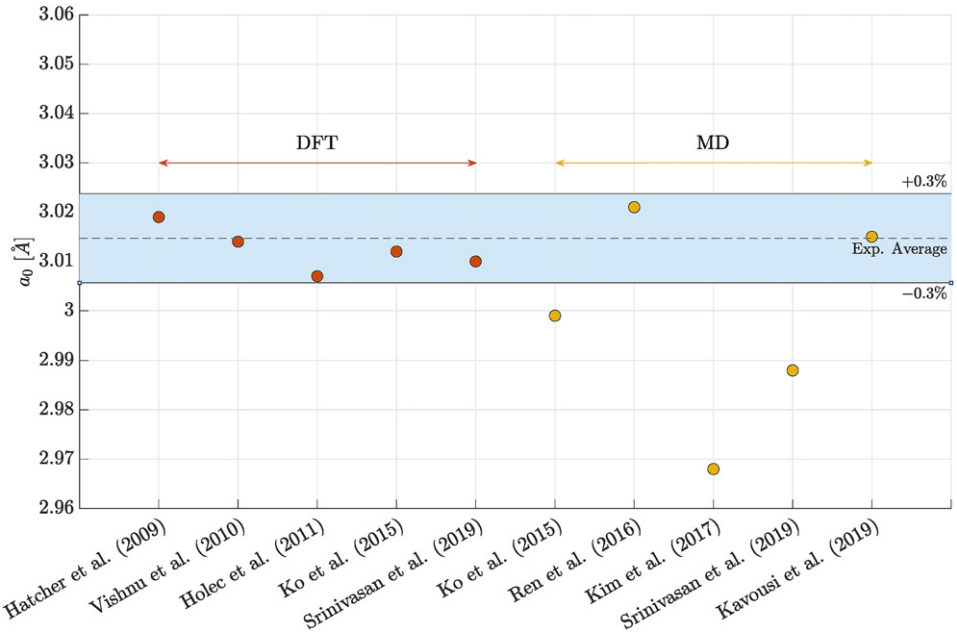

Figure 6. DFT and MD predictions of the B2 lattice parameter, compared with the experimental range.

and Sehitoglu 2016, Kim *et al* 2017, Srinivasan *et al* 2019, Kavousi *et al* 2019) Ni–Ti lattice parameters, compared with the experimental range determined in figures 1–3.

Figure 6 shows that DFT atomistic simulations are well contained within the $\pm 0.3\%$ experimental range error from the average B2 lattice parameter, yet MD simulations are typically outside, in fact Ko *et al* (2015) shows an error of -0.52%, while Kim *et al* (2017) and Srinivasan *et al* (2017) show an error of -1.55% and -0.88%, respectively. It is worth noting that Kavousi *et al* (2019) 2NN-MEAM IAP accurately predicts the B2 lattice parameter (error $+0.01\%$).

Figure 7 reports the atomistic simulation predictions for the B19′ martensite, that are compared with the experimental bounds from figures 2 and 3.

Figure 7 shows that, with only one notable exception (Srinivasan *et al* (2019)), atomistic calculations poorly predict most of the lattice parameters and monoclinic angle of the B19′ crystal structure. In some cases, DFT predictions can be more inaccurate than MD IAPs. Among the DFT lattice parameters shown in figure 7, the calculations closest to experiments have been provided by Hatcher *et al* (2009a,b) and Srinivasan *et al* (2019), who have achieved an acceptable accuracy for the a lattice parameter ($+0.92\%$ and $+0.68\%$ errors) and the monoclinic angle β ($+\ 0.92\%$ error in both cases). The largest mismatch is found in Ko *et al* (2015) DFT predictions. Ko *et al* (2015) prediction of β suggests a B19″ structure (Vishnu and Strachan (2010)) rather than B19′. Vishnu and Strachan (2010) claimed, with DFT calculations, that the B19″ phase can exhibit shape memory, however, to the best of the authors' knowledge, this crystal structure has not been observed experimentally. Figure 7 confirms that the RF-MEAM IAP (Srinivasan *et al* 2019) outperforms both EAM (Ren and Sehitoglu 2016) and 2NN-MEAM (Ko *et al* 2015, Kim *et al* 2017, Kavousi *et al* 2019) and can capture all the lattice parameters of the martensitic cell with remarkable accuracy, with respect to the experimental observations.

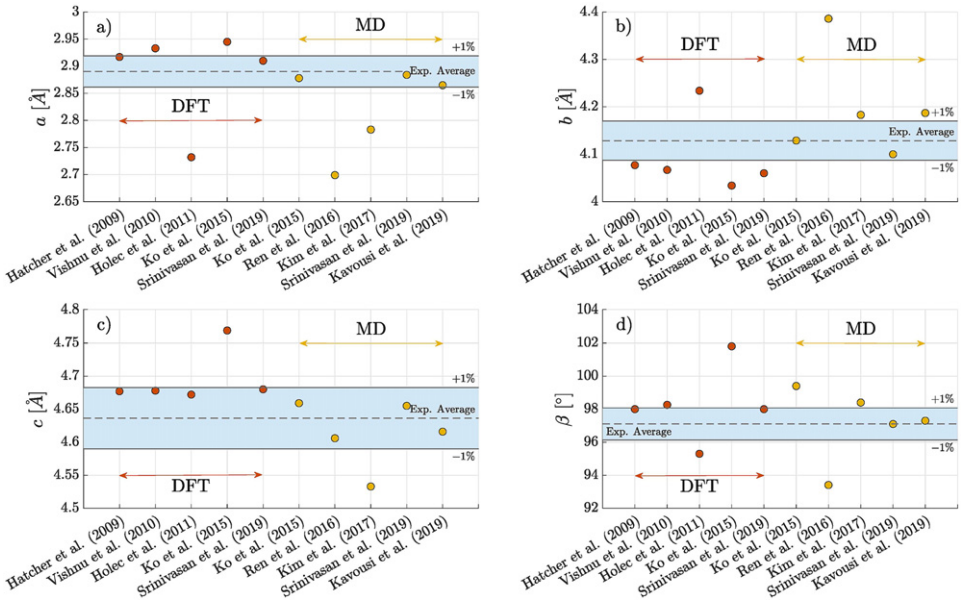

Figure 7. DFT and MD predictions for the B19′ the (a) a, (b) b, (c) c lattice parameters and the (d) monoclinic angle β, compared with the experimental range.

On the contrary, it is clear that Ren and Sehitoglu (2016) FS IAP is rather inaccurate in its description of the B19′ phase, with errors up to -6.62% for a, $+6.23\%$ for b and -3.80% for β. Despite the fact that Ren and Sehitoglu (2016) fitted their potential to a large set of energies and elastic constants obtained *ab initio* or experimentally, their predictions are less accurate than all other potentials considered here, because Ren and Sehitoglu (2016) used the FS formalism, while all the other potentials were developed within the MEAM setting. However, both Ko *et al* (2015) and Srinivasan *et al* (2019) MEAM potentials, that are fitted to a DFT database, perform better than semiempirical IAPs. Unlike DFT calculations, Ko *et al* (2015) IAP predicts all the lattice parameters very accurately, except for the monoclinic angle β that shows a $+2.37\%$ mismatch. Building on the IAP developed by Ko *et al* (2015), Kavousi *et al* (2019) developed a new IAP based on the 2NN-MEAM formalism. The parameters of Kavousi *et al* (2019) IAP were obtained by adjusting them, through a trial-and-error process, using the initial values of the corresponding parameters developed by Ko *et al* (2015). The result of this optimisation process seems to give good accuracy in the prediction of the lattice parameters (except for b, $+1.44\%$ error). Finally, it is unclear why Srinivasan *et al* (2019) MD calculations are in better agreement with experiments than the DFT data they have been fitted to.

We now focus on the prediction of the martensite microstructure, by using as input data for equations (2) and (8) the DFT and MD lattice parameters of the B2 and B19′ phases, that are listed in table 4.

Figure 8 shows the EMT predictions in terms of twinning system (type II mode B twin) and habit plane, with the lattice parameters showed in table 4.

Except Holec *et al* (2011), EMT predictions based on DFT lattice parameters capture well some aspects of the twinning. Hatcher *et al* (2009a,b), Vishnu and Strachan (2010), Srinivasan *et al* (2019) predict accurately the shape strain magnitude and the volume change, and the twin volume fractions are very close to the $\pm 9\%$ range. Instead, the twinning shear predictions are outside the experimental range.

Table 4. Set of B2 and B19′ lattice parameters, from DFT and MD IAPs.

	a_0 (Å)	a (Å)	b (Å)	c (Å)	β (°)	$\Delta V/V_0(\%)$
Hatcher *et al* (2009a,b) (DFT)	3.019	2.917	4.077	4.677	98.00	+0.09
Vishnu and Strachan (2010) (DFT)	3.014	2.933	4.067	4.678	98.26	+0.85
Holec *et al* (2011) (DFT)	3.007	2.732	4.234	4.672	95.30	−1.04
Ko *et al* (2015) (DFT)	3.012	2.945	4.034	4.769	101.80	+1.48
Srinivasan *et al* (2019) (DFT)	3.010	2.910	4.060	4.680	98.00	+0.39
Ko *et al* (2015) (MD)	2.999	2.878	4.129	4.659	99.40	+1.25
Ren and Sehitoglu (2016) (MD)	3.021	2.699	4.386	4.606	93.41	−1.29
Kim *et al* (2017) (MD)	2.968	2.783	4.183	4.533	98.40	−0.17
Srinivasan *et al* (2019) (MD)	2.988	2.884	4.100	4.655	97.10	+2.37
Kavousi *et al* (2019) (MD)	3.015	2.865	4.187	4.616	97.30	+0.20

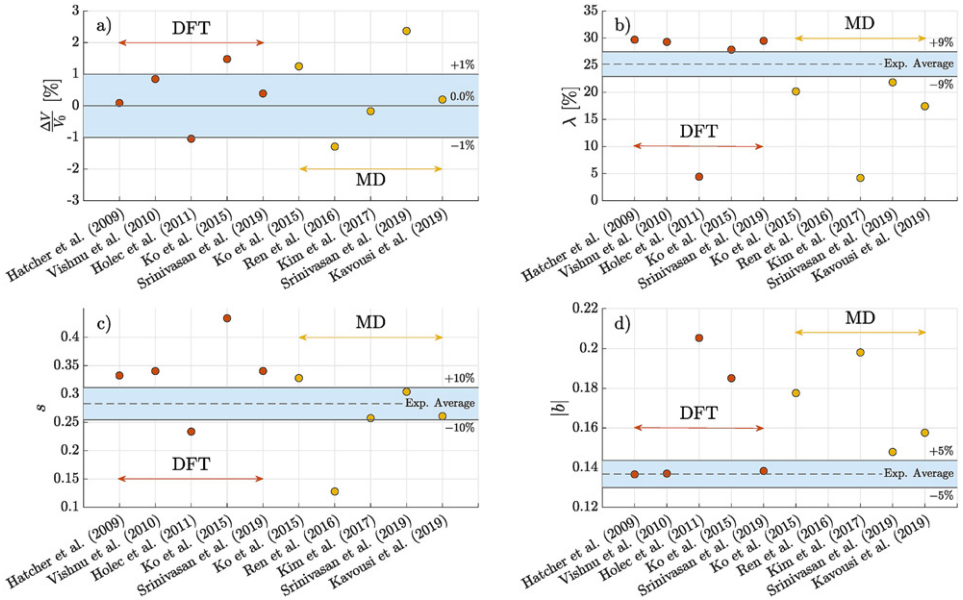

Figure 8. EMT predictions of (a) volume change, (b) twin volume fraction, (c) twinning shear and (d) shape strain magnitude, by using lattice parameters taken from atomistics. Here, only the results for type II mode B twinning systems are shown.

Turning to MD, Srinivasan *et al* (2019) MD predictions on the volume change lie outside the experimental range (+2.37%). The reason is that the volume change depends on both the B2 and B19′ cell structures. Despite predicting B19′ accurately, Srinivasan *et al* (2019) underpredict the B2 lattice parameter, hence the mismatch. Nevertheless, the Srinivasan *et al* (2019) potential remains the best in terms of both twinning shear s and shape strain magnitude $|b|$. As for the twin volume fraction λ, no IAP falls within the experimental range and the most accurate is still the Srinivasan *et al* (2019) IAP (−13.33% error).

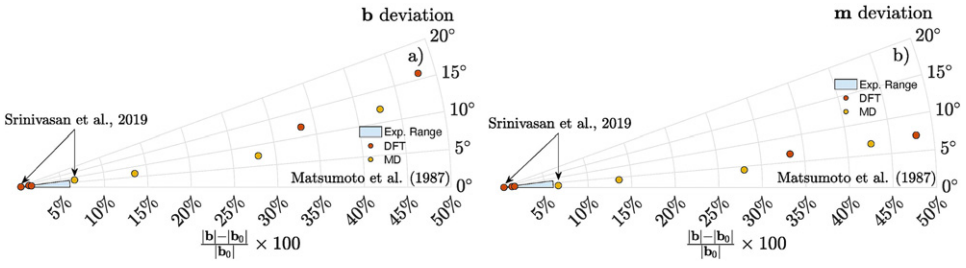

Figure 9. Deviation of the (a) shape strain direction and magnitude and (b) the habit plane normal direction and shape strain magnitude from Matsumoto *et al* (1987) measurements, by using lattice parameters from atomistic simulations. $|\mathbf{b}_0|$ is the Matsumoto *et al* (1987) shape strain magnitude.

Ren and Sehitoglu (2016) IAP predictions of the twinning shear (error -54.79%) are extremely inaccurate, however this is not the most striking aspect. In fact, figure 8 does not show either λ or $|b|$, with Ren and Sehitoglu (2016) lattice parameters, because they do not meet the conditions (equation (9)) since $\delta = 0.55 > -2$. This yields unphysical solutions ($\lambda = -0.5759$) for equation (8).

Figure 9 shows the EMT predictions of the habit plane orientation, compared with the Matsumoto *et al* (1987) measurements.

DFT predictions based on Hatcher *et al* (2009a,b) and Srinivasan *et al* (2019) fall within the experimental range, both in the case of the shape strain (5.67° and 5.92° deviations, respectively) and the habit plane normal (5.12° and 4.32° deviations, respectively). However, DFT predictions based on Holec *et al* (2011) and Ko *et al* (2015) are far from the experimental bounds, with deviations of 15.85° and 11.91°, for the shape strain vector **b**, and 7.17° and 6.65°, for the habit plane normal **m**, respectively.

Predictions based on IAPs for MD are typically less accurate than the DFT ones. Srinivasan *et al* (2019) and Kavousi *et al* (2019) predictions are the closest to experiments for both the shape strain (7.22° and 6.68° deviations, respectively) and the habit plane normal (2.05° and 3.79° deviations, respectively). However the shape strain magnitudes differ form Matsumoto *et al* (1987) by $+7\%$ and $+14\%$, respectively. The, Ko *et al* (2015) and Kim *et al* (2017) predictions are inaccurate in terms of shape strain direction (7.45° and 12.09° deviations, respectively) and shape strain magnitude ($+28\%$ and $+43\%$, respectively).

4. Discussion and conclusions

In this work, we have proposed a methodology for assessing the accuracy of IAPs for the simulation of microstructure in SMAs, by considering the specific case of Ni–Ti. Guided by EMT (Ball and James 1987), that shows that the microstructure of the martensite depends on the austenite and martensite lattice parameters, we assess the sensitivity of the predicted twinning structures and the austenite/martensite interfaces with respect to uncertainties in the experimental input. This approach reveals the striking sensitivity of the EMT predictions on the input lattice parameters, and the need to assess IAPs for atomistic simulations based on their ability to predict the microstructural features (twinning and habit planes). Unlike previous conclusions by Prokoshkin *et al* (2004), figures 1–3 show that the lattice parameters of both the B2 and B19′ phases depend only weakly on the close-to-equiatomic chemical composition changes and the temperature. The experimental values fall well within a $\pm 1\%$ accuracy margin.

The analysis of the accuracy ranges based on EMT predictions and experimental lattice parameters raises a major problem in the choice of the IAPs for atomistic situations. Indeed, the quality of an IAP is typically tested by 'how close' an IAP reproduces the lattice parameters (Ko *et al* 2015, Ren and Sehitoglu 2016, Kim *et al* 2017, Srinivasan *et al* 2019, Kavousi *et al* 2019), without defining 'how accurate' the IAP predictions should be. However, as shown here, minute variations of the lattice parameter values may induce large changes in twin volume fraction, twinning shear and shape strain magnitude. The features of the transformation (such as volume change, twinning shear, twin volume fraction and shape strain magnitude) must also be accurately predicted by atomistic simulations, by falling within/close to the experimental ranges shown in figure 4. Hence, the ability of an IAP to predict martensitic microstructures should be verified by using equations (2) and (8) with the lattice parameters of the atomistic model.

Among the existing IAPs for MD simulations, Ren and Sehitoglu (2016) IAP fails both in the description of crystalline phases and of the martensite microstructures, largely underestimating the twinning shear. However, more importantly, the lattice parameters that Ren and Sehitoglu (2016) derive, from atomistic simulations, are unable to produce a compatible interface between B2 austenite and B19′ martensite, since the conditions set out in equation (9) are not satisfied.

From the present analysis, we can conclude that, among all the IAPs developed for the equiatomic Ni–Ti alloys and analysed here, Srinivasan *et al* (2019) is the IAP that best describes both the martensite crystal structure and the martensite microstructure of twins and habit planes. The main problem lies in the underestimation of the B2 lattice parameter, which, however, does not influence the microstructural predictions, which lie within/close to the experimental range. Another IAP that yields predictions close to the experimental range is the one developed by Kavousi *et al* (2019), which succeeds in describing the austenitic phase very well, but is slightly less accurate than that of Srinivasan *et al* (2019) when it comes to describing the martensitic phase. Regarding the description of the microstructure, although the accuracy is far less than that of the Srinivasan *et al* (2019) IAP, the results are close to experiments.

With the methodology for evaluating IAPs introduced here, we have shown that any IAP must be such that its lattice parameters are not only accurate within the experimental range, but also capable of producing the observed microstructure of martensite. Thus, a necessary (but not sufficient) condition for any sets of lattice parameters, predicted by atomistic simulations, is to satisfy the conditions shown in equation (9). The fulfillment of the conditions (9) implies constraints on the possible choices of the lattice parameters and the monoclinic angle β, and we found that the first condition, on the δ parameter, is the most stringent one. The conditions (9) and the comparison with the experimental bounds determined in this work can guide the development of IAPs that predict accurately the microstructure of martensite.

As a final note, we observe that many IAPs, especially those based on machine learning (ML) approaches, are fitted to large databases of DFT-calculated atomistic configurations. Our analysis shows that DFT calculations could also fall short in predicting accurately the features of martensite, therefore care should be taken when setting up the DFT simulations to create the databases for fitting the ML potentials.

Table 5. Experimental values of the Ni–Ti B2 austenite lattice parameter as a function of chemistry and observation temperature.

	Ni (at.%)	T_{obs} (K)	a_0 (Å)
Otsuka *et al* (1971a)	49.75	293	3.015
Sittner *et al* (2003)	50.50	300	3.0125
Prokoshkin *et al* (2004)	50.00	393	3.0203 ± 0.0008
Prokoshkin *et al* (2004)	50.00	323	3.0175 ± 0.0007
Prokoshkin *et al* (2004)	50.00	293	3.0164 ± 0.0006
Prokoshkin *et al* (2004)	50.70	393	3.0164 ± 0.0008
Prokoshkin *et al* (2004)	50.70	293	3.0121 ± 0.0007
Prokoshkin *et al* (2004)	50.70	261	3.0107 ± 0.0007
Khalil-Allafi *et al* (2004)	50.70	294	3.0141 ± 0.0006
Khalil-Allafi *et al* (2004)	50.70	331	3.01595 ± 0.00003
Khalil-Allafi *et al* (2004)	50.70	347	3.01658 ± 0.00003
Khalil-Allafi *et al* (2004)	50.70	235	3.0069 ± 0.0004
Khalil-Allafi *et al* (2004)	50.70	265	3.0093 ± 0.0001
Khalil-Allafi *et al* (2004)	50.10	338	3.0166 ± 0.0001
Khalil-Allafi *et al* (2004)	50.10	348	3.0173 ± 0.0002
Khalil-Allafi *et al* (2004)	50.10	358	3.0176 ± 0.0001

Acknowledgments

This research was supported by the start-up grant of FM at the Faculty of Science and Engineering at the University of Groningen.

Data availability statement

All data that support the findings of this study are included within the article (and any supplementary files).

Appendix

See tables 5 and 6.

Table 6. Experimental measurements of the lattice parameters of Ni–Ti B19′ martensite, as a function of the composition and temperature. The ⋆ means that the listed values have been recalculated by Prokoshkin *et al* (2004).

	Ni (at.%)	T_{obs} (K)	a (Å)	b (Å)	c (Å)	β (°)
Dautovich and Purdy (1965) ⋆	49.75	296	2.8700 ± 0.0100	4.1100 ± 0.0300	4.6000 ± 0.0300	97.40 ± 0.40
De Lange and Zijderveld (1968) ⋆	50.00	293	2.9040 ± 0.0050	4.1210 ± 0.0020	4.6490 ± 0.0060	97.90 ± 0.10
Otsuka *et al* (1971a) ⋆	49.75	81	2.8740 ± 0.0060	4.1130 ± 0.0090	4.6300 ± 0.0090	97.00 ± 0.10
Otsuka *et al* (1971b) ⋆	49.75	220	2.8800 ± 0.0050	4.1480 ± 0.0020	4.6210 ± 0.0030	96.40 ± 0.10
Otsuka *et al* (1971b) ⋆	49.75	95	2.8720 ± 0.0030	4.1240 ± 0.0020	4.6320 ± 0.0030	96.90 ± 0.10
Hehemann and Sandrock (1971)	50.50	—	2.8830 ± 0.0040	4.1170 ± 0.0050	4.6230 ± 0.0050	96.80 ± 1.00
Monasevich *et al* (1979)	49.80	293	2.8930	4.1200	4.6570	97.60
Monasevich and Paskal (1980)	50.30	293	2.8890	4.1200	4.6220	96.80
Tadaki and Wayman (1980) ⋆	50.00	293	2.9090 ± 0.0070	4.1410 ± 0.0030	4.6390 ± 0.0050	96.80 ± 0.20
Michal and Sinclair (1981)	50.00	—	2.8850	4.1200	4.6220	96.80
Buhrer *et al* (1983)	49.20	10	2.8840	4.1100	4.6650	98.10
Savvinov *et al* (1984) ⋆	51.00	228	2.8870 ± 0.0030	4.1140 ± 0.0030	4.6340 ± 0.0020	96.70 ± 0.10
Savvinov *et al* (1984) ⋆	51.00	123	2.8980 ± 0.0040	4.1430 ± 0.0020	4.6530 ± 0.0030	97.30 ± 0.10
Kudoh *et al* (1985)	49.20	293	2.8980	4.1080	4.6460	97.78
Khachin *et al* (1992)	48.50	293	2.9000	4.1100	4.6600	97.80
Khachin *et al* (1992)	50.00	293	2.8900	4.1200	4.6400	97.30
Khachin *et al* (1992)	50.50	223	2.8900	4.1500	4.6400	97.10
Khachin *et al* (1992)	51.00	123	2.8900	4.1400	4.6500	97.10
Mironov and Kul'Kov (1994) ⋆	50.10	294	2.9040 ± 0.0040	4.1410 ± 0.0030	4.6540 ± 0.0030	97.10 ± 0.10
Mironov and Kul'Kov (1994)	50.10	347	2.9020 ± 0.0060	4.1550 ± 0.0030	4.6320 ± 0.0030	96.60 ± 0.10
Gundyrev *et al* (1999) ⋆	50.50	293	2.8860 ± 0.0030	4.1380 ± 0.0020	4.6290 ± 0.0020	96.70 ± 0.10
Gundyrev *et al* (1999) ⋆	50.50	253	2.8830 ± 0.0030	4.1320 ± 0.0030	4.6360 ± 0.0030	96.90 ± 0.10
Lukas *et al* (2002)	50.50	202	2.8815	4.1232	4.6256	97.00
Prokoshkin *et al* (2004)	50.00	293	2.9090 ± 0.0030	4.1135 ± 0.0035	4.6570 ± 0.0035	97.90 ± 0.10
Prokoshkin *et al* (2004)	50.70	293	2.8820 ± 0.0040	4.1430 ± 0.0050	4.6140 ± 0.0060	96.35 ± 0.15
Prokoshkin *et al* (2004)	50.00	323	2.9100 ± 0.0030	4.1230 ± 0.0035	4.6540 ± 0.0035	97.80 ± 0.10
Prokoshkin *et al* (2004)	50.70	261	2.8820 ± 0.0040	4.1280 ± 0.0050	4.6230 ± 0.0060	96.70 ± 0.15

(*continued on next page*)

Table 6. Continued

	Ni (at.%)	T_{obs} (K)	a (Å)	b (Å)	c (Å)	β (°)
Khalil-Allafi *et al* (2004)	50.70	245	2.8934 ± 0.0004	4.1270 ± 0.0003	4.6354 ± 0.0006	97.18 ± 0.02
Khalil-Allafi *et al* (2004)	50.70	294	2.8930 ± 0.0010	4.1340 ± 0.0010	4.6330 ± 0.0010	96.96 ± 0.03
Khalil-Allafi *et al* (2004)	50.70	298	2.8964 ± 0.0005	4.1351 ± 0.0004	4.6234 ± 0.0007	96.76 ± 0.02
Khalil-Allafi *et al* (2004)	50.70	235	2.8786 ± 0.0002	4.1340 ± 0.0002	4.6215 ± 0.0004	96.65 ± 0.01
Khalil-Allafi *et al* (2004)	50.70	265	2.8792 ± 0.0002	4.1394 ± 0.0002	4.6140 ± 0.0003	96.47 ± 0.01

ORCID iDs

L La Rosa https://orcid.org/0000-0003-1123-7567
F Maresca https://orcid.org/0000-0002-3858-2267

References

Ball J M and James R D 1987 Fine phase mixtures as minimizers of energy *Arch. Ration. Mech. Anal.* **100** 13–52
Baskes M I 1992 Modified embedded-atom potentials for cubic materials and impurities *Phys. Rev.* B **46** 2727
Bhadeshia H K D H and Wayman C M 2014 Phase transformations: nondiffusive *Physical Metallurgy* (Amsterdam: Elsevier) pp 1021–72
Bhattacharya K 1992 Self-accommodation in martensite *Arch. Ration. Mech. Anal.* **120** 201–44
Bhattacharya K 2003 *Microstructure of Martensite: Why it Forms and How it Gives Rise to the Shape-Memory Effect* (*Oxford Series on Materials Modelling* vol 2) (Oxford: Oxford University Press)
Bil C, Massey K and Abdullah E J 2013 Wing morphing control with shape memory alloy actuators *J. Intell. Mater. Syst. Struct.* **24** 879–98
Bilby B A and Crocker A 1965 The theory of the crystallography of deformation twinning *Proc. R. Soc.* A **288** 240–55
Buehler W J, Gilfrich J V and Wiley R C 1963 Effect of low-temperature phase changes on the mechanical properties of alloys near composition TiNi *J. Appl. Phys.* **34** 1475–7
Buhrer W, Gotthardt R, Kulik A, Mercier O and Staub F 1983 Powder neutron diffraction study of nickel–titanium martensite *J. Phys. F: Met. Phys.* **13** L77
Dautovich D P and Purdy G R 1965 Phase transformations in TiNi *Can. Metall. Q.* **4** 129–43
Daw M S and Baskes M I 1984 Embedded-atom method: derivation and application to impurities, surfaces, and other defects in metals *Phys. Rev.* B **29** 6443
De Lange R G and Zijderveld J A 1968 Shape-memory effect and the martensitic transformation of TiNi *J. Appl. Phys.* **39** 2195–200
Duerig T, Pelton A and Stöckel D 1999 An overview of nitinol medical applications *Mater. Sci. Eng.* A **273–275** 149–60
Duwez P and Taylor J L 1950 The structure of intermediate phases in alloys of titanium with iron, cobalt, and nickel *JOM* **2** 1173–6
Ezaz T, Sehitoglu H and Maier H J 2011 Energetics of twinning in martensitic NiTi *Acta Mater.* **59** 5893–904
Farkas D, Roqueta D, Vilette A and Ternes K 1996 Atomistic simulations in ternary Ni–Ti–Al alloys *Modelling Simul. Mater. Sci. Eng.* **4** 359
Finnis M W and Sinclair J E 1984 A simple empirical N-body potential for transition metals *Phil. Mag.* A **50** 45–55
Fujita H and Toshiyoshi H 1998 Micro actuators and their applications *Microelectron. J.* **29** 637–40
Furuya Y 1996 Design and material evaluation of shape memory composites *J. Intell. Mater. Syst. Struct.* **7** 321–30
Furuya Y and Shimada H 1991 Shape memory actuators for robotic applications *Mater. Des.* **12** 21–8
Gundyrev V M, Zel'Dovich V I and Sobyanina G A 1999 Texture and thermal expansion anomalies of B19′-martensite in tensile deformed TiNi shape memory alloy *Textures Microstruct.* **32** 529283
Hane K F and Shield T W 1999 Microstructure in the cubic to monoclinic transition in titanium–nickel shape memory alloys *Acta Mater.* **47** 2603–17
Hartl D J and Lagoudas D C 2007 Aerospace applications of shape memory alloys *Proc. Inst. Mech. Eng.* G **221** 535–52
Hatcher N, Kontsevoi O Y and Freeman A J 2009a Martensitic transformation path of NiTi *Phys. Rev.* B **79** 020202
Hatcher N, Kontsevoi O Y and Freeman A J 2009b Role of elastic and shear stabilities in the martensitic transformation path of NiTi *Phys. Rev.* B **80** 144203
Hautcoeur A and Eberhardt A 1997 Eyeglass frame with very high recoverable deformability *US Patent* 5640217

Hehemann R F and Sandrock G D 1971 Relations between the premartensitic instability and the martensite structure in TiNi *Scr. Metall.* **5** 801–5
Holec D, Friák M, Dlouhý A and Neugebauer J 2011 *Ab initio* study of pressure stabilized NiTi allotropes: pressure-induced transformations and hysteresis loops *Phys. Rev.* B **84** 224119
Ishida H and Hiwatari Y 2007 MD simulation of martensitic transformations in TiNi alloys with meam *Mol. Simul.* **33** 459–61
Jani J M, Leary M and Subic A 2014 Shape memory alloys in automotive applications *Applied Mechanics and Materials* vol 663 (Switzerland: Trans Tech Publications) pp 248–53
Kahn H, Huff M A and Heuer A H 1998 The TiNi shape-memory alloy and its applications for MEMS *J. Micromech. Microeng.* **8** 213
Kavousi S, Novak B R, Baskes M I, Zaeem M A and Moldovan D 2019 Modified embedded-atom method potential for high-temperature crystal-melt properties of Ti–Ni alloys and its application to phase field simulation of solidification *Modelling Simul. Mater. Sci. Eng.* **28** 015006
Khachin V N, Pushin V G and Kondrat'ev V V 1992 Titanium nickelide: structure and properties *Nauka* (in Russian)
Khalil-Allafi J, Schmahl W W, Wagner M, Sitepu H, Toebbens D and Eggeler G 2004 The influence of temperature on lattice parameters of coexisting phases in NiTi shape memory alloys—a neutron diffraction study *Mater. Sci. Eng.* A **378** 161–4
Kheirikhah M M, Rabiee S and Edalat M E 2010 A review of shape memory alloy actuators in robotics *Robot Soccer World Cup* (Berlin: Springer) pp 206–17
Kim Y-K, Kim H-K, Jung W-S and Lee B-J 2017 Development and application of Ni–Ti and Ni–Al–Ti 2NN-MEAM interatomic potentials for Ni-base superalloys *Comput. Mater. Sci.* **139** 225–33
Knowles K M and Smith D A 1981 The crystallography of the martensitic transformation in equiatomic nickel–titanium *Acta Metall.* **29** 101–10
Ko W-S, Grabowski B and Neugebauer J 2015 Development and application of a Ni–Ti interatomic potential with high predictive accuracy of the martensitic phase transition *Phys. Rev.* B **92** 134107
Kudoh Y, Tokonami M, Miyazaki S and Otsuka K 1985 Crystal structure of the martensite in Ti-49.2 at.% Ni alloy analyzed by the single crystal x-ray diffraction method *Acta Metall.* **33** 2049–56
Lai W S and Liu B X 2000 Lattice stability of some Ni–Ti alloy phases versus their chemical composition and disordering *J. Phys.: Condens. Matter* **12** L53
Laves F and Wallbaum H J 1939 Zur Kristallchemie von Titan-Legierungen *Naturwissenschaften* **27** 674–5
Leo D J, Weddle C, Naganathan G and Buckley S J 1998 Vehicular applications of smart material systems *Smart Structures and Materials 1998: Industrial and Commercial Applications of Smart Structures Technologies* vol 3326 (International Society for Optics and Photonics) pp 106–16
Lukas P, Sittner P, Neov D, Novák V, Lugovyy D and Tovar M 2002 R-phase phenomena in neutron diffraction investigations of thermomechanically loaded NiTi polycrystals *Materials Science Forum* vol 404 (Switzerland: Trans Tech Publications Ltd) pp 835–40
Machado L G and Savi M A 2003 Medical applications of shape memory alloys *Braz. J. Med. Biol. Res.* **36** 683–91
Mantovani D 2000 Shape memory alloys: properties and biomedical applications *JOM* **52** 36–44
Matsumoto O, Miyazaki S, Otsuka K and Tamura H 1987 Crystallography of martensitic transformation in ti-ni single crystals *Acta Metall.* **35** 2137–44
Michal G M and Sinclair R 1981 The structure of TiNi martensite *Acta Crystallogr.* B **37** 1803–7
Mironov Y P and Kul'kov S N 1994 Motion picture x-ray diffraction investigation of the martensitic transformation in nickel–titanium alloy *Russ. Phys. J.* **37** 741–5
Monasevich L A, Borisova S D and Paskal Y L 1979 Crystallogeometry of structural phase transitions in titanium nickelide *Izv. vuz. Fiz.* 33 (in Russian)
Monasevich L A and Paskal Yu I 1980 'Martensite–martensite' transformation in titanium nickelide *Fiz. Met. Metalloved.* **49** 813-7 (in Russian)
Morgan N B 2004 Medical shape memory alloy applications—the market and its products *Mater. Sci. Eng.* A **378** 16–23
Muralles M, Park S-D, Kim S Y and Lee B 2017 Phase transformations, detwinning and superelasticity of shape-memory NiTi from MEAM with practical capability *Comput. Mater. Sci.* **130** 138–43
Mutter D and Nielaba P 2010 Simulation of structural phase transitions in NiTi *Phys. Rev.* B **82** 224201
Nishida M, Ohgi H, Itai I, Chiba A and Yamauchi K 1995a Electron microscopy studies of twin morphologies in B19′ martensite in the Ti–Ni shape memory alloy *Acta Metall. Mater.* **43** 1219–27

Nishida M, Wayman C and Chiba A 1988 Electron microscopy studies of the martensitic transformation in an aged Ti-51 at% Ni shape memory alloy *Metallography* **21** 275–91
Nishida M, Yamauchi K, Itai I, Ohgi H and Chiba A 1995b High resolution electron microscopy studies of twin boundary structures in B19′ martensite in the Ti–Ni shape memory alloy *Acta Metall. Mater.* **43** 1229–34
Ölander A 1932 An electrochemical investigation of solid cadmium–gold alloys *J. Am. Chem. Soc.* **54** 3819–33
Onda T, Bando Y, Ohba T and Otsuka K 1992 Electron microscopy study of twins in martensite in a Ti-50.0 at% Ni alloy *Mater. Trans. JIM* **33** 354–9
Otsuka K and Kakeshita T 2002 Science and technology of shape-memory alloys: new developments *MRS Bull.* **27** 91–100
Otsuka K and Ren X 2005 Physical metallurgy of Ti–Ni-based shape memory alloys *Prog. Mater. Sci.* **50** 511–678
Otsuka K, Sawamura T and Shimizu K 1971a Crystal structure and internal defects of equiatomic TiNi martensite *Phys. Status Solidi a* **5** 457–70
Otsuka K, Sawamura T, Shimizu K and Wayman C M 1971b Characteristics of the martensitic transformation in TiNi and the memory effect *Metall. Trans.* **2** 2583–8
Petrini L and Migliavacca F 2011 Biomedical applications of shape memory alloys *J. Metall.* **2011** 501483
Philip T V and Beck P A 1957 CsCL-type ordered structures in binary alloys of transition elements *JOM* **9** 1269–71
Prokoshkin S D, Korotitskiy A V, Brailovski V, Turenne S, Khmelevskaya I Y and Trubitsyna I B 2004 On the lattice parameters of phases in binary Ti–Ni shape memory alloys *Acta Mater.* **52** 4479–92
Purdy G R and Parr J G 1960 A study of T; e titanium–nickel system between Ti_2Ni and TiNi *Technical Report* (OntarioMcMaster University)
Ren G and Sehitoglu H 2016 Interatomic potential for the NiTi alloy and its application *Comput. Mater. Sci.* **123** 19–25
Saitoh K-i, Kubota K and Sato T 2010 Atomic-level structural change in Ni–ti alloys under martensite and amorphous transformations *Tech. Mech.* **30** 269–79
Savvinov A S, Sivokha V P, Voronin V P and Khachin V N 1984 Structure transition in titanium–nickelide-based alloys *Izv. vuz. Fiz.* 17 (in Russian)
Schetky L M 1991 Shape memory alloy applications in space systems *Mater. Des.* **12** 29–32
Sehitoglu H, Karaman I, Anderson R, Zhang X, Gall K, Maier H J and Chumlyakov Y 2000 Compressive response of NiTi single crystals *Acta Mater.* **48** 3311–26
Sittner P, Lukás P, Neov D, Novák V and Toebbens D M 2003 *In situ* neutron diffraction studies of martensitic transformations in NiTi *J. Phys. IV* **112** 709–11
Song C 2010 History and current situation of shape memory alloys devices for minimally invasive surgery *Open Med. Dev. J.* **2** 24–31
Sreekumar M, Nagarajan T, Singaperumal M, Zoppi M and Molfino R 2007 Critical review of current trends in shape memory alloy actuators for intelligent robots *Ind. Robot* **34** 285–94
Srinivasan P, Duff A I, Mellan T A, Sluiter M H F, Nicola L and Simone A 2019 The effectiveness of reference-free modified embedded atom method potentials demonstrated for NiTi and NbMoTaW *Modelling Simul. Mater. Sci. Eng.* **27** 065013
Srinivasan P, Nicola L and Simone A 2017 Modeling pseudo-elasticity in NiTi: why the meam potential outperforms the EAM-FS potential *Comput. Mater. Sci.* **134** 145–52
Stoeckel D 1990 Shape memory actuators for automotive applications *Mater. Des.* **11** 302–7
Tadaki T and Wayman C M 1980 Crystal structure and microstructure of a cold worked TiNi alloy with unusual elastic behavior *Scr. Metall.* **14** 911–4
Timonova M and Thijsse B J 2010 Optimizing the MEAM potential for silicon *Modelling Simul. Mater. Sci. Eng.* **19** 015003
Van Humbeeck J 1999 Non-medical applications of shape memory alloys *Mater. Sci. Eng.* A **273–275** 134–48
Vishnu K G and Strachan A 2010 Phase stability and transformations in NiTi from density functional theory calculations *Acta Mater.* **58** 745–52
Vishnu K G and Strachan A 2012 Size effects in NiTi from density functional theory calculations *Phys. Rev.* B **85** 014114
Wayman C M 1994 The phenomenological theory of martensite crystallography: interrelationships *Metall. Mater. Trans.* A **25** 1787–95

Wu M H and Schetky L M 2000 Industrial applications for shape memory alloys *Proc. Int. Conf. Shape Memory and Superelastic Technologies* vol 44, p 1 (Pacific Grove, California)

Zhong Y, Gall K and Zhu T 2011 Atomistic study of nanotwins in NiTi shape memory alloys *J. Appl. Phys.* **110** 033532

Zider R B and Krumme J F 1988 Eyeglass frame including shape-memory elements *US Patent* 4772112